

All ion fragmentation analysis enhances the untargeted profiling of glucosinolates in *Brassica* microgreens by liquid chromatography and high-resolution mass spectrometry

Andrea Castellaneta¹, Ilario Losito^{1,2,*}, Giovanni Cisternino¹, Beniamino Leoni³, Pietro Santamaria^{2,3}, Cosima Damiana Calvano^{1,2}, Giuliana Bianco⁴, Tommaso R.I. Cataldi^{1,2}

¹Dipartimento di Chimica, ²Centro Interdipartimentale SMART, ³Dipartimento di Scienze Agro-Ambientali e Territoriali, Università degli Studi di Bari Aldo Moro, via Orabona 4, 70126 Bari, Italy; ⁴Dipartimento di Scienze, Università degli Studi della Basilicata, viale dell'Ateneo Lucano 10, 85100 Potenza, Italy.

ABSTRACT: An analytical approach based on reversed-phase liquid chromatography coupled to electrospray ionization Fourier-transform mass spectrometry in negative ion mode (RPLC-ESI(-)-FTMS) was developed for the untargeted characterization of glucosinolates (GSL) in the polar extracts of four *Brassica* microgreen crops, namely garden cress, rapeseed, kale, and broccoli raab. Specifically, the *all ion fragmentation* (AIF) operation mode enabled by a quadrupole-Orbitrap mass spectrometer, *i.e.*, the systematic fragmentation of all ions generated in the electrospray source, followed by the acquisition of an FTMS spectrum, was exploited. First, the best qualifying product ions for GSL were recognized from higher-energy collisional dissociation (HCD)-FTMS² spectra of representative standard GSL. Extracted ion chromatograms (EIC) were subsequently obtained for those ions from RPLC-ESI(-)-AIF-FTMS data referred to microgreen extracts, by plotting the intensity of their signals as a function of retention time. The alignment of peaks detected in the EIC traces was finally exploited for the recognition of peaks potentially related to GSL, with the EIC obtained for the sulphate radical anion [SO₄]⁻ (exact *m/z* 95.9523) providing the highest selectivity. Each putative GSL was subsequently characterized by HCD-FTMS² analyses and by collisionally induced dissociation (CID) multistage MSⁿ (*n* = 2,3) acquisitions based on a linear ion trap mass spectrometer. As a result, up to 27 different GSLs were identified in the four *Brassica* microgreens. The general method described in this work appears as a promising approach for the study of GSL, known and novel, in plant extracts.

INTRODUCTION

The health benefits associated with the consumption of *Brassica* vegetables (also known as *Cruciferous*) were already known in ancient Rome (“*Brassica est, quae omnibus holeribus antistat*”, Cato, *De re Rustica De Agri Cultura*)¹ and still represent a major driving force for their worldwide production, along with their distinctive flavour and aroma^{2,3}. Particularly, *Brassica* crops are rich sources of glucosinolates (GSL), sulphur-rich secondary metabolites acting as precursors of a variety of bioactive compounds involved in plant defense⁴⁻⁶. As shown in **Figure 1**, all GSL share a common structural motif, consisting of a β-thioglucopyranose moiety, whose S atom is linked to the C atom involved in the C=N group of a sulfated oxime. The same C atom binds a distinctive R side group for each GSL, with the C=N bond of the oxime having a *Z* configuration⁷. R groups of GSL resemble those of amino acids acting as their biosynthetic precursors, thus they are usually classified into three main groups, namely aliphatic (*i.e.*, GSL arising from methionine, alanine, leucine, isoleucine, and valine), benzenic (GSL generated by phenylalanine and tyrosine) and indolic (tryptophan derivatives)⁸.

Upon cutting or mastication of vegetal tissues, thioglucosidase enzymes known as myrosinases^{4,6} are released and catalyse

the conversion of glucosinolates into their unstable aglycones. Further catabolites, like epithionitriles, isothiocyanates, nitriles and thiocyanates⁸ are subsequently formed from

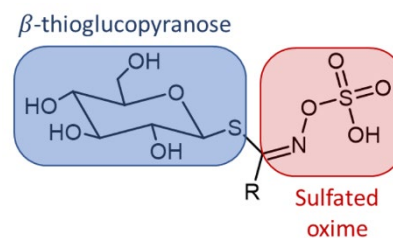


Figure 1. General molecular structure of glucosinolates

aglycones and have been reported to play a role in preventing cancer, cardiovascular diseases, and other inflammatory disorders⁹.

Since glucosinolates can be subjected to thermal degradation when vegetables are cooked¹⁰, microgreens of *Brassica* species, that can be consumed as raw foodstuff, have emerged as a potentially relevant source of these compounds. Here, the

term “microgreens” refers to young and tender edible seedlings usually harvested at the soil level a few days after germination, when the cotyledons are fully expanded and still turgid¹¹. Microgreens have been recently claimed as novel “superfoods” by virtue of their content in nutritional and bioactive compounds^{12,13}.

Due to their structural diversity, the examination of the

GSL profile in plant extracts requires reliable and high-throughput analytical methods. Although the quantitative analysis of desulfo-glucosinolates (des-GSL) based on ISO 9167:2019 is still considered a conventional method for the characterization of GSL^{6,10}, it implies complex and time-consuming sample treatments, including purification on anion exchanger cartridges and implementation of the enzymatic desulfation reaction. Moreover, the determination of des-GSL is impaired by the lack of analytical standards for all GSL^{6,9,14}. Mass spectrometry (MS)-based analysis of intact glucosinolates has been proven to be more consistent and timesaving if compared to the conventional analysis of their desulphated derivatives¹⁰. The easy formation of deprotonated molecules ($[M-H]^-$) by electrospray ionization (ESI), the distinctive isotope pattern, related to the presence of two sulphur atoms in their structure, and the occurrence of specific fragmentation pathways during MS² analyses have contributed to the success of mass spectrometry in GSL analysis¹⁵⁻¹⁶. ESI-MS² data of GSL obtained by an ion trap were exploited by Rochfort *et al.*¹⁷ for the development of a rapid qualitative screening method for GSL in infused plant extracts. Nevertheless, the coupling between liquid chromatography (LC) and MS detection leads to a more robust GSL identification and has been recently applied also to desulphated GSL¹⁸. In this context, reversed-phase liquid chromatography (RPLC) has been widely employed for the separation of GSL¹⁴. Although proposed as a possible alternative¹⁹, hydrophilic interaction liquid chromatography (HILIC) may suffer from chromatographic interferences introduced by ion clusters²⁰ arising from salts occurring in the plant extracts. Looking at the MS detection, the possible presence of several co-extracted phytochemicals makes high-resolution mass spectrometry (HRMS) a very interesting tool for the untargeted profiling of GSL. Very recently, two LC-HRMS methods, based on mass defect (MDF)²¹ and modified-Kendrick mass defect (MKD)²² have been proposed.

Alternatively, the so-called *all ion fragmentation* (AIF) operation mode, *i.e.*, the fragmentation of ionized analytes without any prior precursor ion selection, recently employed in our laboratory in the lipidomics context²³, may provide a powerful option to extend the GSL profiling of vegetal extracts based on HRMS analysis. Indeed, as previously mentioned, deprotonated GSL show common fragmentation pathways, leading to well-defined product ions²¹, potentially useful as qualifier ions. In this work, extracted ion chromatograms (EICs) obtained from RPLC-ESI(-) FTMS data resulting from AIF acquisitions and focusing on specific GSL product ions were used to detect GSL in *Brassica* microgreen extracts. The identity of each GSL was confirmed by accurate m/z values, isotope pattern evaluation and the synergic interpretation of targeted HCD-FTMS² and CID-MSⁿ (with $n = 2, 3$) data, obtained using a quadrupole-Orbitrap and a linear ion trap (LIT) mass spectrometer, respectively. If available, the direct comparison of chromatographic and mass spectrometric features of standard compounds was

exploited to improve the confidence level for GSL structure identification, as suggested by Schymanski *et al.*²⁴.

The proposed approach was employed for the systematic GSL profiling of four *Brassica* microgreen crops, namely garden cress, rapeseed, kale, and broccoli raab.

EXPERIMENTAL

Chemicals

LC-MS grade acetonitrile, water, and methanol, analytical grade acetone and HPLC grade hexane, used for RPLC separations and/or GSL extraction, and formic acid (LC-MS grade), employed as mobile phase additive, were purchased from Merck (Milan, Italy). Standards of prop-2-enyl (sinigrin), (2R)-2-hydroxybut-3-enyl (progoitrin), indol-3-ylmethyl (glucobrassicin) and 4-(methylsulfinyl)butyl GSL (glucoraphanin) were purchased from Merck (Milan, Italy).

Microgreen production

Microgreens were grown using seeds of garden cress (*Lepidium sativum* L., cv. Crescione dei Giardini), broccoli raab (*Brassica rapa* L. subsp. *sylvestris* L. Janch. var. *esculenta* Hort., cv. Novantina), rapeseed (*Brassica napus* L., cv. PR44D06) and kale (*Brassica oleracea* var. *acephala*, cv. Landrace). Seeds for the former three species were purchased, respectively, from local farms “Riccardo Larosa” and “Tesoro della Terra” (Andria, Italy) and Pioneer Hi-Bred Italia Sementi (Sissa, Italy). Kale seeds were produced in a university greenhouse. Details on the experimental conditions adopted for microgreens growth are reported in Section S1 of the Supporting Information. Harvesting of microgreens was carried out once the appearance of the first true leaves was assessed, namely, after 17 days for garden cress and broccoli raab, 18 days for kale and 22 days for rapeseed. The seedlings were cut just above the surface of the growing medium, stored for two days at -20 °C and then freeze-dried for four days in a ScanVac CoolSafe 55-9 Pro-freeze-dryer (LaboGene ApS, Lyngø, Denmark).

Extraction of glucosinolates and sample preparation

The extraction of glucosinolates was based on the protocol proposed by Cataldi *et al.*⁷, integrated with a purification step aimed at removing vegetal proteins. Specifically, 200 mg of lyophilized microgreens were powdered using a mortar. The resulting powder was suspended in 3 mL of a CH₃OH/H₂O 70:30 (v/v) solution and incubated at 75 °C for 10 min. Thereafter, the mixture was sonicated at 40 °C for 10 min using a DU-32 ultrasonic bath (Argo Lab, Carpi, Italy), working at 40 kHz. After centrifugation (10 min at 4500 g), the supernatant was recovered, and the extraction procedure was repeated on the solid residue. As described in Section S2 and Figure S1 of the Supporting Information, the use of two extraction steps enabled the achievement of recoveries close to 90% for most glucosinolates occurring in microgreens of broccoli raab and kale, chosen as test matrices since they included the highest numbers of different GSL among the four microgreens under study.

The supernatants resulting from the two extractions steps were pooled and washed with 2.5 mL of hexane to remove the most hydrophobic compounds (*e.g.*, pigments, free fatty acids, etc.). The protocol proposed by De Ceglie *et al.*²⁵, with some modifications, was subsequently used for protein precipitation (see Section S3 of the Supporting Information). The dry residue

of the supernatant obtained after protein precipitation, containing GSL, was dissolved into 5 mL of the CH₃OH/H₂O 70:30 (v/v) mixture and stored in a screw-cap vial. Each extract was diluted by a 1:10 factor (v/v) with LC-MS water before RPLC-ESI(-)-MS analyses.

RPLC-ESI-MS instrumentations and operating conditions

The RPLC-ESI(-)-MS analysis was performed using two LC-MS platforms, both implementing an Ultimate 3000 HPLC quaternary chromatographic system. One of them included a Q-Exactive high-resolution quadrupole-Orbitrap mass spectrometer (Thermo Fisher, West Palm Beach, CA, USA), that was used for Fourier-transform MS (FTMS) and HCD-MS² analyses. The other platform included a Velos Pro low resolution, double-stage linear ion trap mass spectrometer (Thermo Fisher, West Palm Beach, CA, USA), employed for collisionally-induced dissociation (CID) MSⁿ (n = 2,3) acquisitions. In both cases, the chromatographic column effluent was transferred into the heated electrospray ionization (HESI) interface (Thermo Fisher, West Palm Beach, CA, USA) mounted on each mass spectrometer.

RPLC separations were performed using a C18 Ascentis Express column (15 cm length, 2.1 mm internal diameter) packed with core-shell 2.6 μm particles (Supelco, Bellefonte, PA, USA) and operated at a 0.20 mL/min flow; 5 μL sample volumes were injected. The following multi-step binary elution gradient, based on water as phase A and acetonitrile as phase B, both containing 0.1% (v/v) formic acid, was adopted for GSL separation: 0-2 min) isocratic at 1% B; 2-3 min) linear increase of B from 1% to 2%; 3- min) isocratic at 2% B; 5-10 min) linear increase of B from 2% to 10%; 10-20 min) linear increase of B from 10% to 30%; 20-30 min) linear increase of B from 30% to 80%; 30-40 min) isocratic at 80% B; 40-50 min) linear decrease of B from 80% to 1%; 50-60 min) reconditioning at 1% B.

The parameters of the HESI interface and the ion optics of the Q-Exactive spectrometer were set as follows: sheath gas flow rate) 40 a.u.; auxiliary gas flow rate) 15 a.u.; spray voltage) -3 kV; capillary temperature) 320 °C; S-lens RF Level) 60. The spectrometer was operated at its maximum resolving power (140000 at *m/z* 200) and high-resolution spectra were acquired in a 300-700 *m/z* interval. AIF acquisitions were performed at 70000 resolving power in a 50-700 *m/z* interval, using a normalized collisional energy (NCE) of 35 units. The latter was also adopted for targeted HCD-FTMS² acquisitions on GSL ions. In this case, only the monoisotopic mass corresponding to each GSL ion was selected by the spectrometer quadrupole before proceeding with fragmentation in the HCD cell. During MS measurements the Orbitrap fill time was set to 100 ms and the Automatic Gain Control (AGC) level was set as 1 × 10⁶. The spectrometer was calibrated daily by infusing, at a 5 μL/min flow rate, calibration solutions provided by the instrument manufacturer for positive or negative polarity acquisitions. As a result, a mass accuracy always better than 5 ppm was achieved.

The main operating parameters of the Velos Pro spectrometer HESI source and ion optics were set as follows: sheath gas flow rate) 40 a.u.; auxiliary gas flow rate) 15 a.u.; spray voltage) -3 kV; capillary temperature) 350 °C; S-lens RF Level) 60. During MS experiments, the linear ion trap fill time was set to 10 ms and the AGC Level was set as 3 × 10⁴. Collisionally Induced Dissociation (CID) MS² and MS³ spectra were acquired in negative ion mode using a 1 *m/z* wide window to select the monoisotopic mass of the precursor ion and the product ion of interest,

respectively. The normalized collision energy (NCE) for MSⁿ (n=2,3) experiments was set at 40 units.

RESULTS AND DISCUSSION

Recognition of peaks putatively related to GSL using alternated Full MS/AIF analysis

As illustrated in the Total Ion Current (TIC) chromatograms generated by RPLC-ESI(-)-FTMS from kale (see **Figure 2A**), and from broccoli raab, garden cress, and rapeseed microgreen extracts (see **Figure S2** in the Supporting Information), several peaks were detected. On the other hand, EICs could be obtained for GSL typical product ions by reporting the intensity of signals related to their exact *m/z* ratios, retrieved from RPLC-ESI(-)-AIF-FTMS data, as a function of retention time. The EICs referred to two diagnostic product ions of GSL, *i.e.*, those with *m/z* 95.9523 and 259.0129 (*vide infra*), are reported in panels B and C of **Figure 2**. As emphasized in the figure, the alignment of EICs with the TIC chromatogram enabled the recognition of peaks putatively referred to GSL occurring in the kale microgreen extract.

The identification of GSL was confirmed through further steps, leading to identification confidence levels as those suggested by Schymanski *et al.*²⁴. Firstly, ESI(-)-FTMS mass spectra acquired during the elution of each chromatographic peak were averaged and the resulting spectrum was subtracted from the background spectra averaged on retention time intervals located at both sides of the same peak. The peak intensity profiles of isotopologues were subsequently evaluated in the resulting spectrum, searching for profiles including a relatively intense peak for the M+2 isotopologue, potentially related to GSL species. Accurate *m/z* values of monoisotopic (M+0) peaks in those profiles were then employed to retrieve information about the corresponding molecular formulas using the *Qual Browser* routine in the Xcalibur software. Only singly charged even electron (EE) anions were considered, setting a mass accuracy threshold of 5 ppm and the minimum numbers of C, H, N, S and O atoms as 7, 11, 1, 2 and 9, respectively, corresponding to those included in the common molecular skeleton of GSL. The outcomes were compared with the molecular formulas of glucosinolates hosted in the METLIN database (<https://metlin.scripps.edu/>) and with those corresponding to GSL reported in the comprehensive review by Blazevic *et al.*²⁶, including a list of 156 compounds. At least one putative GSL was always recovered.

It is worth noting that the unequivocal knowledge of the molecular formula corresponds to an identification level 4 in the classification given by Schymanski *et al.*²⁴, in which the number referred to each level is decreased with the increase of the identification confidence. By combining the information based on retention time values and the interpretation of targeted HCD-FTMS² and CID-MSⁿ (n = 2,3) spectra (*vide infra*), the identification level for GSL could subsequently be raised to levels 1, 2 or 3, according to the case. In particular, level 3 (*tentative candidate*²⁴) was reached when positional isomers or diastereoisomers could be proposed but MSⁿ data were unable to clarify which of them was present since product ions were not influenced by those types of isomerism. Level 2 (*probable structure*²⁴) was achieved when fragmentation pathways clarified which of the possible positional isomers was present. Finally, level 1 (*confirmed structure*²⁴) was obtained when the

identification of a specific GSL could be confirmed through the comparison of its chromatographic and mass spectrometric features with those of a standard GSL.

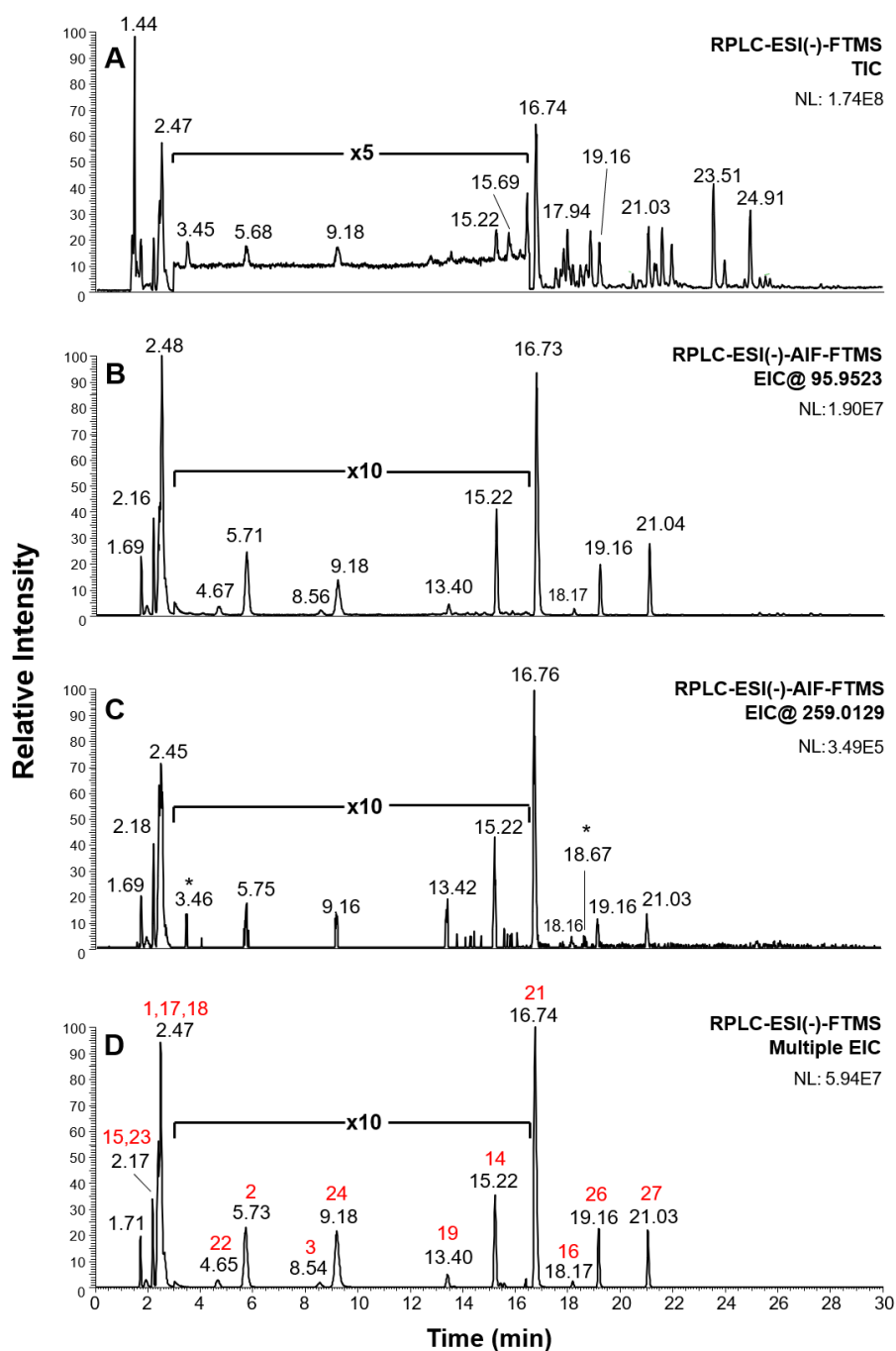


Figure 2. (A) Total ion current chromatogram resulting from RPLC-ESI(-)-FTMS of a kale microgreen extract. (B) Extracted ion chromatogram (EIC) obtained by RPLC-ESI(-)-AIF-FTMS for the GSL product ion corresponding to sulphate radical anion ($[\text{SO}_4]^-$ at m/z 95.9523). (C) EIC obtained by RPLC-ESI(-)-AIF-FTMS for the glucose sulphate anion ($[\text{C}_6\text{H}_{11}\text{O}_9\text{S}]^-$ at m/z 259.0129). (D) Multiple EIC obtained by summing and plotting versus retention time the intensity of signals related to the $[\text{M}-\text{H}]^-$ ions of all GSL identified in kale microgreen extracts (see Table 1). Red numbers correspond to GSL numbers reported in Table 1. NL indicates the signal intensity used for normalization in each chromatogram.

Choice of diagnostic product ions for ion current extraction from RPLC-ESI(-)-AIF-FTMS chromatograms

As anticipated above, the fragmentation of GSL $[M-H]^-$ ions leads to class-specific product ions. This feature was observed also when HCD-FTMS² spectra were acquired for selected GSL, such as glucobrassicin (indol-3-ylmethyl GSL) and neoglucobrassicin (1-methoxyindol-3-ylmethyl GSL), as evidenced in **Figure 3**, panels A and B, respectively. In both cases, tandem MS spectra were dominated by peak signals generated from the gas-phase formation of ions related to the sulphate moiety, *i.e.*, the hydrogen sulphate ion ($[HSO_4]^-$, exact m/z 96.9601) and the sulphate radical anion $[SO_4]^-$ (exact m/z 95.9523), whose structures are reported in **Figure S3** of the Supporting Information. Moreover, the sulphite radical anion ($[SO_3]^-$, exact m/z 79.9574), supposedly generated from the hydrogen sulphate ion²⁷, and a product ion corresponding to the anion of 2-hydroxy-ethylene thiol ($[C_2H_3SO]^-$, exact m/z 74.9910), arising from fragmentation of the thioglucose moiety²⁷ (see **Figure S3**), were detected.

Since the hydrogen sulphate ion was always the base peak in the HCD-FTMS² spectra of deprotonated GSL, the extraction of its current from RPLC-ESI(-)-AIF-FTMS traces was hypothesised to ensure the highest sensitivity in the recognition of GSL. However, the fragmentation of organic sulphate esters might also lead to the formation of the same ion via a six-membered cyclic *syn*-elimination mechanism²⁸, thus generating a possible interference with GSL recognition. Conversely, the gas-phase generation of the sulphate radical anion, $[SO_4]^-$, at m/z 95.9523, would need more strict structural requirements to occur, namely the stabilization of the neutral radical arising from its release. The relevance of the sulphate radical anion as a diagnostic fragment for GSL is evidenced in **Figure 2** by the comparison of its EIC (see panel B) with the one referred to the product ion at m/z 259.0129 (corresponding to glucose sulphate, see **Figure S3**), reported in panels C. The two chromatograms were obtained from the RPLC-ESI(-)-AIF-FTMS data referred to a kale microgreen extract. Moreover, panel D of the same figure reports a multiple EIC, obtained by retrieving, from spectra acquired during the RPLC-ESI(-)-FTMS analysis based on Full MS acquisitions, the intensities of signals related to the $[M-H]^-$ ions of all GSL recognized in the kale microgreen extract, and then summing them and plotting their sum as a function of retention time. This type of EIC can provide a snapshot of all GSL species detected in a specific microgreen extract. As emphasized by magnified sections in panels B and C of **Figure 2**, a higher number of peaks was recognized in the EIC obtained for the sulphate radical anion. In particular, peaks corresponding to GSL subsequently labelled as 3 and 22 (see **Table 1**) were recognized only in that EIC and a much better S/N ratio was observed for peaks detected between 13 and 16 min, where GSL labelled as 14 and 19 were subsequently identified. Moreover, two weak peaks, eluting after 3.46 and 18.5 min (see peaks marked by an asterisk in **Figure 2C**) and observed only in the EIC obtained for the m/z 259.0129 ion, were not confirmed to correspond to any GSL, as emphasized by the comparison with the multiple EIC reported in **Figure 2D**.

Notably, EICs obtained for other typical GSL product ions reported in **Figure S3** were also aligned with those shown in panels B and C of **Figure 2**. However, the EIC related to the $[SO_4]^-$ ion remained the most selective, thus suggesting that the generation of this product ion is systematic in the case of GSL,

at least under the high collisional energy regimes enabled by the HCD cell adopted in the present case. Nonetheless, the peak alignment with EICs referred to other typical fragments of GSL can be used to exclude the eventual interference from co-extracted organic compounds including a sulphate moiety and able to generate the $[SO_4]^-$ ion as a fragment. In the present case, the generation and alignment of EICs could be easily performed using the *Xcalibur* software. The latter is also able to overlap different EICs, after normalizing the corresponding signal intensities, yet, for the sake of clarity, normalized EICs were reported separately in **Figure 2**. Notably, to obtain robust results for analyses involving many samples, it would be preferable to use the version focused on small molecules of the software *Skyline*²⁹, freely available on the Internet (skyline.ms/project/home/software/Skyline/begin.view), rather than manual data processing and evaluation of EICs based on *Xcalibur*. In this case, a transition list including the m/z ratios of GLS fragments and LC-MS/MS data obtained with different MS instrumentations would have to be imported, after setting the acquisition method for MS/MS filtering as DIA (*Data Independent Analysis*), that is equivalent to AIF in the *Skyline* context.

As described in the next section, MSⁿ analyses ($n = 2,3$) were employed for an extended characterization of putative GSL recognized in microgreen extracts through the alignment of EICs referred to as specific product ions.

Improving the confidence level in glucosinolate identification using RPLC-ESI-MSⁿ ($n = 2,3$) data

The β -thioglucose residue linked to the C atom included in the C=N moiety represents the main source of product ions usually detected during fragmentation of GSL, at least when relatively low collisional energy regimes are adopted^{17,27,30}. As already mentioned, the structures of the resulting product ions are depicted in **Figure S3** of the Supporting Information, whereas typical neutral losses are described in **Figure S4**, with each pathway labelled with a Greek letter. As emphasized in **Figures 3A** and **3C**, most of the common fragments (see peaks labelled with red asterisks) and neutral losses (see Greek labels) were identified in the CID-MS² spectrum obtained for the $[M-H]^-$ ion of standard glucobrassicin (m/z 447.1). They were present also in the HCD-FTMS² spectrum, although with a much lower abundance compared to the sulphate moiety fragments; a magnification of the vertical scale was thus required to evidence their formation. The detection of class-specific signals raised the confidence level of GSL identification in microgreen extracts up to level 3, according to the Schymanski classification²⁴. In the presence of isomeric species, additional information was searched for to achieve a higher confidence level in the GSL identification.

As an example, m/z values compatible with the exact m/z ratios 374.0585, potentially referring to isomeric species *n*-butyl, 2-methylpropyl and (1S)-1-methyl-propyl GSL (glucocochlearin), and 402.0898, possibly related to 3-methylpentyl, 4-methylpentyl and *n*-hexyl GSL, were inferred from RPLC-ESI(-)-FTMS analyses (see **Table 1**). As shown in **Figure S5** (Supporting Information), three well-resolved peaks were found in the RPLC-ESI(-)-FTMS EIC chromatograms related to both groups of compounds and obtained for the broccoli raab microgreen extract. Assuming that the retention on the C18 stationary phase of the GSL side chains follows the order

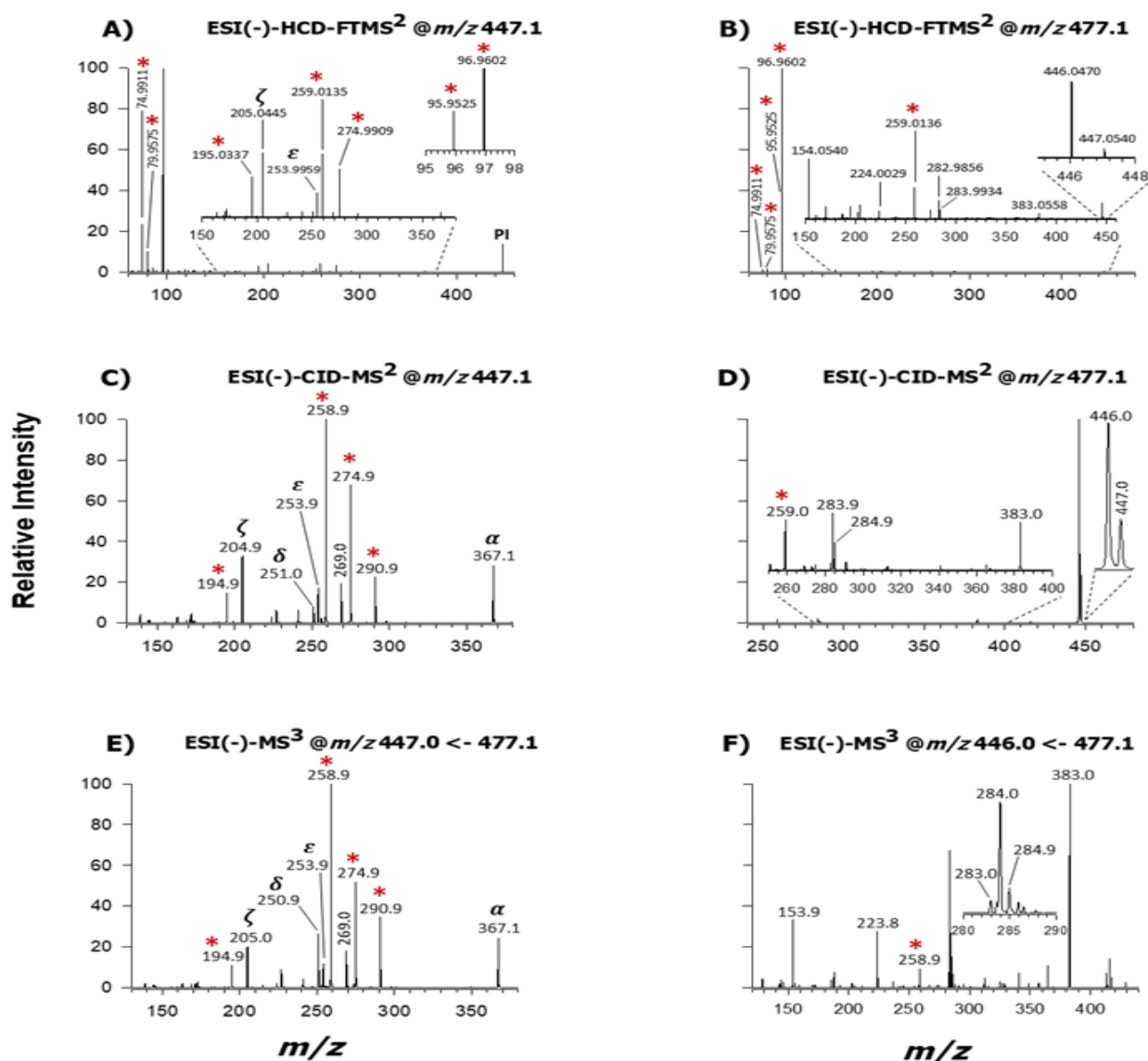


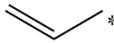
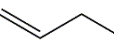
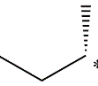

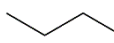
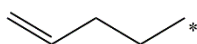
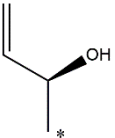
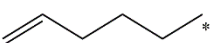
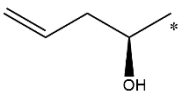
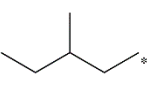
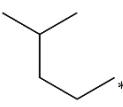
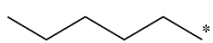
Figure 3. Comparison between ESI(-)-HCD-FTMS² spectra (A, B) and ESI(-)-CID-MS² spectra (C, D) of glucobrassicin (Indol-3-ylmethyl GSL, m/z 447.1) and neoglucobrassicin (N-Methoxyindol-3-ylmethyl GSL, m/z 477.1) $[M-H]^-$ ions. Panels (E) and (F) show the ESI(-)-MS³ spectra referring to the main product ions, at m/z 447.0 and 446.0, respectively, detected in the CID-MS² spectrum of the neoglucobrassicin $[M-H]^-$ ion. Peaks labelled with (*) correspond to diagnostic GSL ions originating from the β -thioglycosylated oxime moiety, whose structures are reported in Figure S3. Peaks labelled with Greek letters refer to common neutral losses of GSL, described in Figure S4. PI = precursor ion. Note that different m/z scales were purposely adopted for some spectra to emphasize the m/z ranges in which relevant signals were detected, thus facilitating the visualization of the latter.

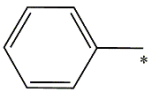
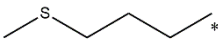
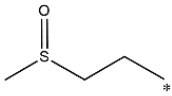
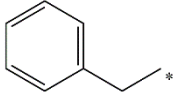
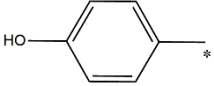
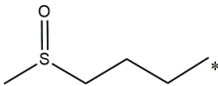
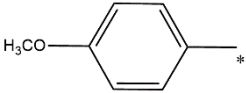
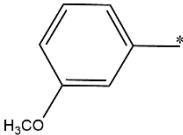
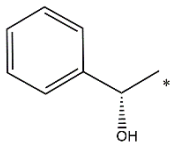
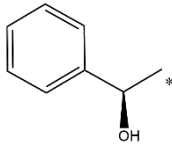
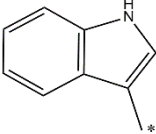
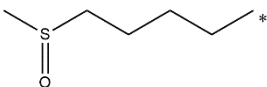
linear > *iso* > *ante iso*, in agreement with Lerario *et al.*³¹, the following retention time order was hypothesised: *n*-butyl > 2-methyl-propyl > 1-methyl-propyl, in one case, and hexyl > 4-methyl-pentyl > 3-methyl-pentyl, in the other case, thus the six GSL were tentatively identified as reported in **Table 1**. Since MS² spectra were not influenced by the side-chain isomerism and standards were not available for each isomeric GSL, these GSL were designated with an identification confidence level of 3. The RPLC method developed during this study also allowed the separation of two methoxylated forms of glucobrassicin, returned by the Metlin database and reported in the literature (see Ref. 26 and references cited therein) as 4-methoxy

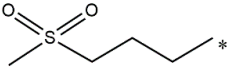
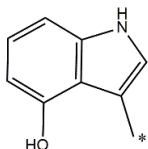
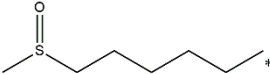
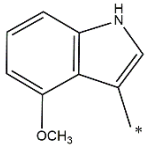
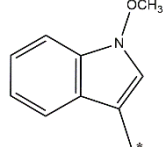
glucobrassicin (4-methoxyindol-3-ylmethyl GSL) and neoglucobrassicin (1-methoxyindol-3-ylmethyl GSL), that were related to peaks 26 and 27, respectively (see **Figure 2D** and **Table 1**). From a chromatographic point of view, it is reasonable to assume a lower polarity, which turns into a higher retention time, for neoglucobrassicin, due to the methoxylation of the heterocyclic N atom, in agreement with previous studies^{21,31}.

It is worth noting that the CID-MS² spectrum of supposed 4-methoxyglucobrassicin at m/z 477.1 (data not shown) was virtually identical to that of glucobrassicin at m/z 447.1 (see **Figure 3C**), excepting for the nominal mass increase of 30 u. Interestingly, the CID-MS² spectrum of putative

Table 1. List of all the glucosinolate (GSL) species detected in microgreens of kale, broccoli raab, garden cress and rapeseed, sorted according to the exact m/z ratios of their $[M-H]^-$ ions. The rational name (and the trivial one, if available) of each GSL, along with the confidence level for structure identification (SCL), according to Schymanski *et al.*²⁸, is reported in the second column, whereas the side chain (R group, see Figure 1) structure is drawn in the third column (with an asterisk indicating the carbon atom linked to the carbon atom of the C=N moiety). Multiple structures are reported for GSL whose chromatographic and mass spectrometric features were unable to provide a more specific identification. The detection of each GSL in the four microgreens investigated is emphasized in the last four columns. ND = not detected.

Peak #	Rational name (trivial name) SCL	R group	$[M-H]^-$ exact m/z value	Occurrence in microgreens extracts			
				Kale	Broccoli raab	Garden cress	Rapeseed
1	Prop-2-enyl GSL (Sinigrin) Level 1		358.0272	+	+	ND	ND
2	But-3-enyl GSL (Gluconapin) Level 2		372.0428	+	+	ND	+
3	(1S)-1-methylpropyl GSL (Glucocochlearin) Level 3		374.0585	+	+	+	+
4	2-methylpropyl GSL Level 3		374.0585	ND	+	ND	ND
5	<i>n</i> -butyl GSL Level 3		374.0585	+	+	+	+
6	Pent-4-enyl GSL (Glucobrassicinapin) Level 2		386.0585	+	+	ND	+
7	(2R)-2-hydroxybut-3-enyl GSL (Progoitrin) Level 1		388.0378	+	+	ND	+
8	5-hexenyl GSL Level 3		400.0741	ND	+	ND	ND
9	(2S)-2-hydroxypent-4-enyl GSL (Gluconapoleiferin) Level 3		402.0534	ND	+	ND	+
10	3-methylpentyl GSL Level 3		402.0898	+	+	ND	+
11	4-methylpentyl GSL Level 3		402.0898	+	+	ND	+
12	<i>n</i> -hexyl GSL Level 3		402.0898	+	+	ND	+

13	Benzyl-GSL (Glucotropaeolin) Level 3		408.0428	+	+	+	+
14	4-(methylthio)-butyl GSL (Glucoerucin) Level 3		420.0462	+	ND	ND	ND
15	3-(methylsulfinyl)-propyl GSL (Glucoiberin) Level 2		422.0255	+	ND	ND	ND
16	2-phenylethyl GSL (Gluconasturtiin) Level 3		422.0585	+	+	ND	+
17	4-hydroxybenzyl GSL (Sinalbin) Level 3		424.0378	ND	ND	+	ND
18	4-(methylsulfinyl)-butyl GSL (Glucoraphanin) Level 1		436.0411	+	ND	ND	+
19	4-methoxybenzyl GSL (Glucoaubrietin) Level 3		438.0534	+	+	ND	+
	3-methoxybenzyl GSL (Glucolimnanthin) Level 3						
20	(2S)-2-hydroxy-2-phenylethyl GSL (Glucobarbarin) Level 3		438.0534	+	+	ND	+
	(2R)-2-hydroxy-2-phenylethyl GSL (Epiglucobarbarin) Level 3						
21	Indol-3-ylmethyl GSL (Glucobrassicin) Level 1		447.0537	+	+	ND	+
22	5-(methylsulfinyl)-pentyl GSL (Glucoalyssin) Level 2		450.0568	+	+	ND	+

23	4-(methylsulfonyl)-butyl GSL (Glucocerysolin) Level 3		452.0360	+	ND	ND	+
24	4-hydroxyindol-3-ylmethyl GSL (4-hydroxy-glucobrassicin) Level 3		463.0487	+	+	ND	+
25	6-(methylsulfinyl)-hexyl GSL (Glucosheperalin) Level 3		464.0724	ND	+	ND	ND
26	4-methoxyindol-3-ylmethyl GSL (4-methoxy-glucobrassicin) Level 3		477.0643	+	+	+	+
27	1-methoxyindol-3-ylmethyl GSL (Neoglucobrassicin) Level 2		477.0643	+	+	ND	+

neoglucobrassicin was remarkably different, being dominated by peaks at m/z 446.0 and 447.0 (see **Figure 3D**), with only one typical GSL fragment detected, as a weak signal, at m/z 259.0. Peak signals at m/z 446.0 and 447.0 were detected, although with a much lower relative abundance, also in the FTMS² spectrum of putative neoglucobrassicin (see the inset in **Figure 3B**) and the corresponding accurate m/z values (446.0470 and 447.0540) enabled their assignment as product ions arising from the neutral losses of a methoxy radical ($\text{CH}_3\text{O}^\bullet$) and a formaldehyde (CH_2O) molecule, respectively. Notably, a product ion with nominal m/z 446.0 was previously detected for neoglucobrassicin and tentatively explained with the methoxy radical loss^{21,32}. In the present case, a confirmation of this hypothesis could be obtained by selecting the m/z 446.0 and 447.0 ions as precursor ions in CID-MS³ acquisitions, performed by the LIT mass spectrometer (see **Figures 3E** and **3F**). Indeed, the CID-MS³ spectrum at m/z 447.0 (panel E) was virtually identical to that of glucobrassicin (panel C). Conversely, the CID-MS³ spectrum of the neoglucobrassicin product ion at m/z 446.0 evidenced the generation of several new product ions, with m/z values 153.9, 223.8, 283.0, 284.0 and 383.0 (see **Figure 3F**). Interestingly, these peaks could all be recognized also in the HCD-FTMS² spectrum of neoglucobrassicin (see **Figure 3B**), although with very low intensity. Their respective accurate m/z ratios, 154.0540, 224.0029, 282.9856, 283.9934 and 383.0558, were useful to hypothesise possible structures for the corresponding product ions, as described in **Figure S6** of the Supporting Information.

In particular, the product ion compatible with an exact m/z 283.9931, along with the one compatible with an exact m/z 259.0129, also detected in the HCD-FTMS² spectrum shown in **Figure 3B**, were explained, respectively, by the neutral loss of dehydrated glucose (see path B in **Figure S6**, corresponding to

the process labelled as β in **Figure S4**) and by the generation of glucose sulphate (see path A in **Figure S6**), which are well-known fragmentation processes of GSL^{27,30}. As far as the other fragments are concerned, a key feature of their possible interpretation was the stability of the indole radical resulting from the neutral loss of the methoxy radical. According to Reva *et al.*³³, electron resonance stabilizes the indole radical by preferentially displacing the unpaired electron from the *N* to the *C3* atom of the indole ring. As described in **Figure S6**, complex pathways initially involving the transfer of one H atom of the $-\text{CH}_2-$ moiety located between the indole ring and the oxime $\text{C}=\text{N}$ group had to be proposed for a tentative explanation of fragments with m/z ratios 154.0540, 224.0029, 282.9856, and 383.0558 detected in the HCD-FTMS² spectrum of neoglucobrassicin. Although a confirmation of those pathways, based on computational studies and/or analyses of isotopically labelled neoglucobrassicin, is needed, the cited fragments appear as specific markers of this GSL. Its identification confidence level was thus reported as 2 in **Table 1**. Unfortunately, fragmentation data were unable to confirm the methoxy group position in the case of 4-methoxyglucobrassicin, for which an identification confidence level equal to 3 was designated in **Table 1**.

By analogy with 4-methoxyglucobrassicin, no loss of the methoxy radical was observed from one of the precursor ions detected at m/z 438.0534, which was compatible with a GSL bearing a methoxy-benzyl side chain (data not shown). Consequently, an indirect confirmation of the linkage of a methoxy group to the benzene ring located on its side chain could be obtained but without establishing its exact position. For this reason, the precursor ion could be related to a couple of methoxybenzyl GSLs reported so far in the literature²⁶, *i.e.*, 4-methoxybenzyl (glucoaubrietin) and 3-methoxybenzyl GSL

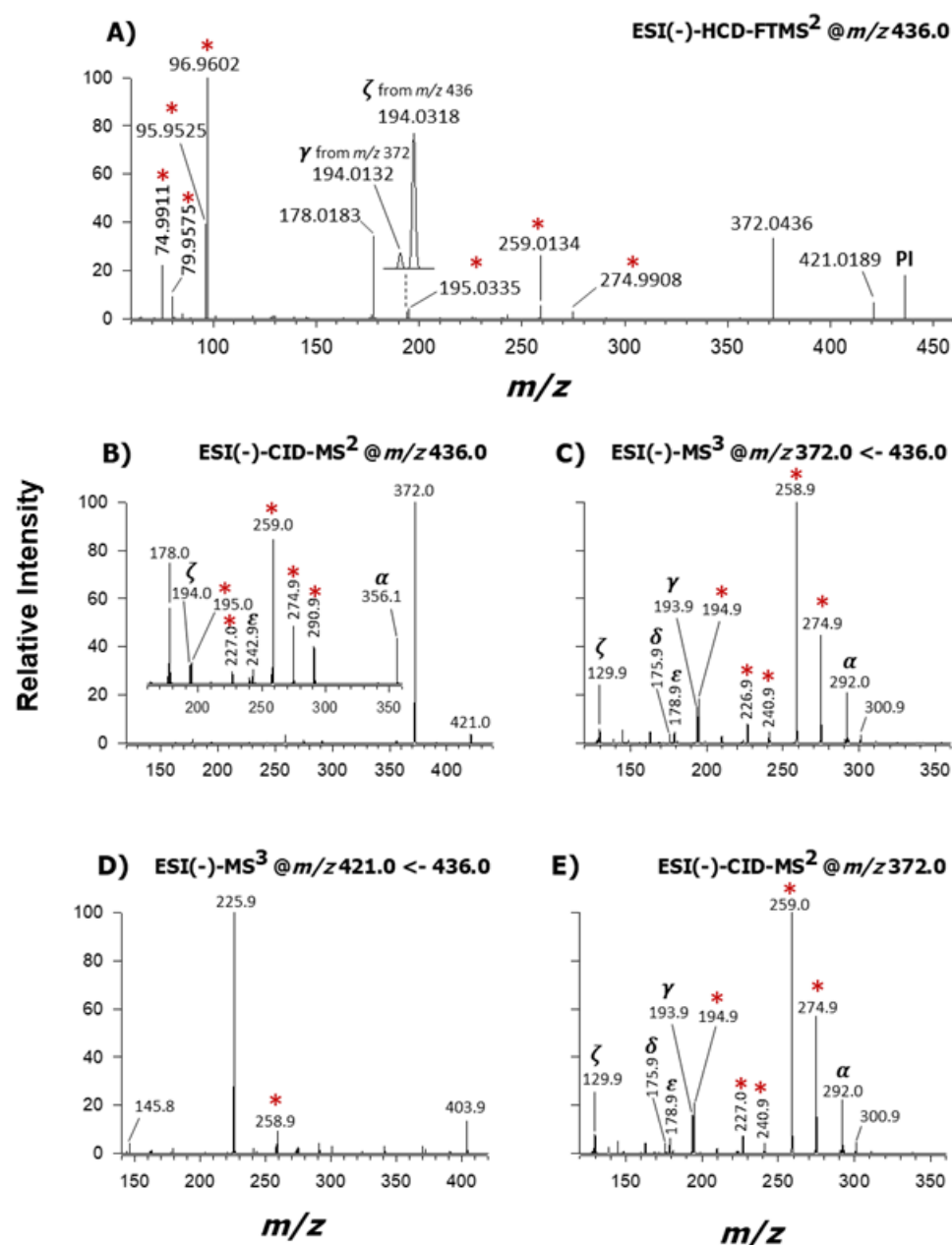


Figure 4. Comparison between (A) ESI(-)-HCD-FTMS² and (B) ESI(-)-CID-MS² spectra of glucoraphanin [M-H]⁻ at m/z 436.0. Panels (C) and (D) show the ESI(-)-MS³ spectra referring to the product ions generated by the neutral loss of a methanesulfenic acid (m/z 372.0) and a methyl radical (m/z 421.0), respectively. Panel (E) shows the ESI(-)-CID-MS² spectrum of but-3-enyl GSL (gluconapin, see Table 1). Peaks labelled with (*) refer to diagnostic GSL ions originating from the β -thioglycosylated oxime moiety, whose structures are reported in Figure S4. Peaks labelled with Greek letters refer to common neutral losses occurring for GSL, described in Figure S5. PI = precursor ion.

(glucolimnanthin), with a level 3 assigned for identification confidence (see GSL #19 in Table 1).

On the other hand, a further putative GSL ion was detected at m/z 438.0534 and a peak whose m/z ratio was compatible with a neutral loss of benzaldehyde, a fragmentation previously reported also by Bianco *et al.*³⁴, was observed in the corresponding MS² spectrum (data not shown). This outcome was in

agreement with the presence of an OH group linked to the ethyl chain located between the benzene ring and the oxime C atom, a structural feature shared by (2S)-2-hydroxy-2-phenylethyl GSL (glucobarbarin) and (2R)-2-hydroxy-2-phenylethyl GSL (epiglucobarbarin). One of these compounds, represented as GSL #20 in Table 1, could thus correspond to the cited precursor ion. Notably, the loss of the aldehyde *acrolein* from the

precursor ion was inferred also from a peak signal detected in the MS² spectrum of the progoitrin [M-H]⁻ ion (data not shown), thus suggesting that the R(Ar)CHO loss is typical of GSL including an R(Ar)CH(OH)CH₂ side chain. In the present case, progoitrin (GSL #7 in **Table 1**) could be identified with a confidence level 1 since a standard was available and no evidence for the additional presence of its isomer epiprogoitrin was obtained from chromatographic data.

As for other GSL detected in the four examined microgreen samples, an identification confidence level 2 was generally achieved for glucosinolates including a saturated side chain ending with the methylsulphinyl (CH₃SO-) group. Nonetheless, a level 1 could be credited to glucoraphanin (GSL #18), among them, upon successfully comparing the retention time and experimental MS² data with those obtained for its commercial standard. The HCD-FTMS² spectrum for its [M-H]⁻ ion (nominal *m/z* 436) is shown in **Figure 4A**. Along with typical product ions of GSL, a relatively intense peak was observed in the spectrum at *m/z* 372.0436, interpreted through the neutral loss of methanesulfenic acid, CH₃SOH (nominal mass 64 u)⁵. The latter was reported as a diagnostic process for all methylsulphinyl GSL²¹. Indeed, the same neutral loss was observed in the HCD-FTMS² spectra of glucoiberin (3-(methylsulfinyl)-propyl GSL, *m/z* 422.0) and glucoalyssin (5-(methylsulfinyl)-pentyl GSL, *m/z* 450.1), reported in **Figures S7A** and **S7C** in the Supporting Information. Notably, the loss of CH₃SOH is expected to generate a glucosinolate having a terminal C=C bond on its side chain, a feature exhibited by other GSL. In the present case, the product ion at *m/z* 372.0436 of glucoraphanin corresponded to the precursor ion of but-3-enyl GSL (gluconapin), another glucosinolate detected in the microgreen extracts (excepting the garden cress one). Not surprisingly, then, the 372.0 ← 436.0 CID-MS³ spectrum for glucoraphanin (see **Figure 4C**) and the CID-MS² spectrum for gluconapin (see **Figure 4E**) were almost identical. Accordingly, the CID-MS³ spectra obtained for [M-H-CH₃SOH]⁻ ions of glucoiberin and glucoalyssin closely resembled the CID-MS² spectra of sinigrin (prop-2-enyl GSL) and glucobrassicinapin (pent-4-enyl GSL), respectively (data not shown).

A further interesting product ion was detected at *m/z* 178.0183 in the HCD-FTMS² spectrum of glucoraphanin (see **Figure 4A**) and, with a much lower intensity, in its CID-MS² spectrum (**Figure 4B**). The ion was not detected in 372 ← 436 and 421 ← 436 CID-MS³ spectra (see **Figures 4C** and **D**), thus suggesting its generation through the loss of a neutral fragment with nominal mass 258 u directly from the precursor ion of glucoraphanin (GSL #18 in **Table 1**) at *m/z* 436.0. As inferred from **Figure S7** in the Supporting Information, the process seemed negligible in the case of the methylsulphinyl GSL glucoiberin (see the peak at *m/z* 164.0023 in **Figure S7A**) and was more likely in the case of glucoalyssin (see the peak at *m/z* 192.0343 in **Figure S7C**). This finding suggested that the length of the side chain of methylsulphinyl GSL affects the probability of that fragmentation. As shown in **Figure S8A** of the Supporting Information, the 258 u neutral loss can be interpreted as the detachment of S-methylsulphinyl-thiogluucose, following a cyclization occurring on the side chain of methylsulphinyl-GSL. The higher stability of 5- and 6-atom rings formed in the case of glucoraphanin and glucoalyssin, compared with the 4-atom ring resulting in the case of glucoiberin, might explain the different intensities observed for the product ions formed upon the loss of S-methylsulphinyl-thiogluucose.

It is worth mentioning that all HCD-FTMS² spectra obtained for methylsulphinyl GSL also exhibited the gas-phase loss of a methyl radical (CH₃[•]), as shown in **Figures 4A**, **S7A** and **S7C**, with the occurrence of peak signals at *m/z* 421.0819, 407.0270 and 435.0349, respectively. As indicated in **Figure S8B** of the Supporting Information, the resulting fragments are alkylsulphinyl radical anions, whose further fragmentation was explored by CID-MS³ experiments, as evidenced in **Figures 4D**, **S7B** and **S7D**. The neutral loss of the hydroxyl radical was recognizable in the fragmentation spectra of the [M-H-CH₃]⁻ ions of glucoraphanin (see the peak signal at *m/z* 403.9 in **Figure 4D**) and glucoalyssin (see the ion at *m/z* 418.0 in **Figure S7D**), whereas the process seemed negligible in the case of glucoiberin. The generation of the remaining main product ions detected in the fragmentation spectra of glucoiberin, glucoraphanin and glucoalyssin [M-H-CH₃]⁻ ions was tentatively explained as illustrated in **Figure S8B**. In this case, the main pathway would consist of an α -hydrogen extraction from the side chain of [M-H-CH₃]⁻ ions, followed by the loss of a thiogluucose radical (with the unpaired electron located on the S atom). The process requires the folding of the side chain of each precursor ion, leading to a cyclic intermediate. The higher stability expected for the 5- or 6-membered cyclic intermediates formed in the case of glucoiberin and glucoraphanin, compared to the 7-membered intermediate related to glucoalyssin, might explain the higher relevance of the thiogluucose radical loss observed from the demethylated precursors of the first two GSL.

In the case of all the remaining GSL listed in **Table 1**, MSⁿ data were unable to support the identification with a confidence level 2, due to the lack of relevant fragmentations involving the GSL side chains. Therefore, a level 3 identification was designed, and the structures reported in **Table 1** correspond to those hosted in the Metlin database or generally reported in the literature²⁶. As easily inferred from the last four columns of **Table 1**, significant differences in the qualitative profile of detected GSL were observed between the four microgreens under study. The garden cress microgreens exhibited a very characteristic profile, with only 5 GSL detected and benzyl-GSL (glucotropaeolin) prevailing among them, at least according to the EIC peak area (data not shown). Up to 20 GSL were detected for rapeseed microgreens and 22 for both kale and broccoli raab ones, with some differences observed between the GSL identified for the three microgreens.

From a more general point of view, despite the much lower number of considered vegetal species, most GSL detected during the present study were included among the 47 species recently reported by Dong *et al.*²¹, whose investigation of 25 different vegetal products represents one of the most extended studies on GLS in *Brassica* microgreens published so far. Interestingly, additional species were detected in the present case, namely, 2-methylpropyl-, *n*-butyl-, 5-hexenyl-, 4-hydroxybenzyl- (sinalbin) and 4-methoxybenzyl GSL (glucoaubrietin). These results support the importance of the AIF analysis in enhancing the investigation of GSL in microgreens and other vegetal matrices as well.

Conclusions

Reversed phase liquid chromatography coupled to high resolution Fourier-transform mass spectrometry performed in the AIF operation mode, *i.e.*, based on the systematic fragmentation of precursor ions in the HCD cell of a quadrupole-Orbitrap mass spectrometer, followed by the acquisition of high-resolution spectra, was proposed as a new approach for the extended untargeted screening of glucosinolates (GSL) in vegetal samples, specifically in *Brassica* microgreen extracts. Chromatographic peaks potentially related to GSL were recognized by generating and aligning extracted ion chromatograms related to some of their typical product ions. Among the latter, the radical sulphate anion ($[\text{SO}_4]^-$, exact m/z 95.9523) emerged as the most selective for the extended recognition of GSL peaks. As a result, 27 GSL were evidenced in the polar extracts of four *Brassica* microgreens. The compounds could be subsequently identified at different confidence levels, with useful structural information being obtained by the synergic use of MS^n data ($n = 2,3$), acquired either in a high (HCD-FTMS²) or in a low (CID-MSⁿ) collisional energy regime. The developed approach appears as a very promising analytical tool for the detailed screening of GSL in all types of vegetable samples. On the other hand, work is underway to obtain quantitative information on GSL recognized in the four *Brassica* microgreens, in the perspective of selecting those containing the largest amounts of beneficial GSL as potential novel foods in the human diet.

ASSOCIATED CONTENT

Supporting Information

The Supporting Information is available free of charge on the ACS Publications website.

- 1) **Section S1.** Experimental conditions adopted for microgreens growth.
- 2) **Section S2.** Evaluation of glucosinolate extraction yield.
- 3) **Figure S1.** Contribution of each of three subsequent steps to the overall extraction yield of GSL from broccoli raab and kale microgreens.
- 4) **Section S3.** Procedure for the removal of vegetal proteins from microgreen extracts.
- 5) **Figure S2.** RPLC-ESI(-)-FTMS total ion current chromatograms referred to extracts of broccoli raab, garden cress, and rape-seed microgreens.
- 6) **Figure S3.** Chemical structures reported in the literature for the most important common product ions resulting from the fragmentation of glucosinolate $[\text{M-H}]^-$ ions.
- 7) **Figure S4.** Neutral losses involving the β -thioglycosylated oxime sulphate moiety are typically observed in the tandem mass spectra of GSL $[\text{M-H}]^-$ ions.
- 8) **Figure S5.** RPLC-ESI(-)-FTMS extracted ion current (EIC) chromatograms obtained for GSL $[\text{M-H}]^-$ ions with m/z 402.0898 (A) and 374.0585 (B) detected in the extracts of broccoli raab microgreens.
- 9) **Figure S6.** Fragmentation pathways hypothesized to explain the generation of specific product ions detected in the HCD-FTMS² spectra of $[\text{M-H}]^-$ ions of neoglucobrassicin and in the CID-MS² and MS³ spectra related to the same glucosinolate.
- 10) **Figure S7.** HCD-FTMS² spectra of $[\text{M-H}]^-$ ions and CID-MS³ spectra of $[\text{M-H-CH}_3]^-$ ions of glucoiberin and glucoalyssin.
- 11) **Figure S8.** Fragmentation pathways hypothesized to explain the generation of some of the most abundant product ions detected in the HCD-FTMS² spectra of $[\text{M-H}]^-$ ions and in the CID-MS³

spectra of $[\text{M-H-CH}_3]^-$ ions of glucoiberin, glucoraphanin, and glucoalyssin.

File type: PDF

AUTHOR INFORMATION

Corresponding Author

* Ilario Losito, University of Bari “Aldo Moro”, Department of Chemistry, e-mail: ilario.losito@uniba.it.

Author Contributions

The manuscript was written with the contributions of all authors. All authors have approved the final version of the manuscript.

ACKNOWLEDGMENT

This work was supported by the following grant: PONa3_00395/1 “Bioscienze & Salute (B&H)”, funded by the Italian *Ministero per l'Istruzione, l'Università e la Ricerca* (MIUR).

REFERENCES

1. Ruhee, R.T.; Suzuki, K.: The Integrative Role of Sulforaphane in Preventing Inflammation, Oxidative Stress and Fatigue: A Review of a Potential Protective Phytochemical. *Antioxidants*. 9, 521 (2020). <https://doi.org/10.3390/antiox9060521>
2. Quirante-Moya, S., García-Ibañez, P., Quirante-Moya, F., Villaño, D., Moreno, D.A.: The Role of Brassica Bioactives on Human Health: Are We Studying It the Right Way? *Molecules*. 25, 1591 (2020). <https://doi.org/10.3390/molecules25071591>
3. Favela-González, K.M., Hernández-Almanza, A.Y., De la Fuente-Salcido, N.M.: The value of bioactive compounds of cruciferous vegetables (Brassica) as antimicrobials and antioxidants: A review. *J. Food Biochem.* 44, (2020). <https://doi.org/10.1111/jfbc.13414>
4. Dinkova-Kostova, A.T., Kostov, R. V.: Glucosinolates and isothiocyanates in health and disease. *Trends Mol. Med.* 18, 337–347 (2012). <https://doi.org/10.1016/j.molmed.2012.04.003>
5. Cataldi, T.R.I., Lelario, F., Orlando, D., Bufo, S.A.: Collision-Induced Dissociation of the A + 2 Isotope Ion Facilitates Glucosinolates Structure Elucidation by Electrospray Ionization-Tandem Mass Spectrometry with a Linear Quadrupole Ion Trap. *Anal. Chem.* 82, 5686–5696 (2010). <https://doi.org/10.1021/ac100703w>
6. Nguyen, V.P.T., Stewart, J., Lopez, M., Ioannou, I., Allais, F.: Glucosinolates: Natural Occurrence, Biosynthesis, Accessibility, Isolation, Structures, and Biological Activities. *Molecules*. 25, 4537 (2020). <https://doi.org/10.3390/molecules25194537>
7. Cataldi, T.R.I., Rubino, A., Lerario, F., Bufo, S.A.: Naturally occurring glucosinolates in plant extracts of rocket salad (*Eruca sativa* L.) identified by liquid chromatography coupled with negative ion electrospray ionization and quadrupole ion-trap mass spectrometry. *Rapid Commun. Mass Spectrom.* 21, 2374–2388 (2007). <https://doi.org/https://doi.org/10.1002/rcm.3101>
8. Sikorska-Zimny, K., Beneduce, L.: The glucosinolates and their bioactive derivatives in Brassica: a review on classification, biosynthesis and content in plant tissues, fate during and after processing, effect on the human organism and interaction with the gut microbiota. *Crit. Rev. Food Sci. Nutr.* 61, 2544–2571 (2021). <https://doi.org/10.1080/10408398.2020.1780193>
9. Almushayti, A.Y., Brandt, K., Carroll, M.A., Scotter, M.J.: Current analytical methods for determination of glucosinolates in vegetables and human tissues. *J. Chromatogr. A*. 1643, 462060 (2021). <https://doi.org/10.1016/j.chroma.2021.462060>
10. Yu, X., He, H., Zhao, X., Liu, G., Hu, L., Cheng, B., Wang, Y.: Determination of 18 Intact Glucosinolates in Brassicaceae

- Vegetables by UHPLC-MS/MS: Comparing Tissue Disruption Methods for Sample Preparation. *Molecules*. 27, 231 (2021). <https://doi.org/10.3390/molecules27010231>
11. Kyriacou, M.C., Roupael, Y., Di Gioia, F., Kyratzis, A., Serio, F., Renna, M., De Pascale, S., Santamaria, P.: Micro-scale vegetable production and the rise of microgreens. *Trends Food Sci. Technol.* 57, 103–115 (2016). <https://doi.org/10.1016/j.tifs.2016.09.005>
 12. Paradiso, V.M., Castellino, M., Renna, M., Gattullo, C.E., Calasso, M., Terzano, R., Allegretta, I., Leoni, B., Caponio, F., Santamaria, P.: Nutritional characterization and shelf-life of packaged microgreens. *Food Funct.* 9, 5629–5640 (2018). <https://doi.org/10.1039/C8FO01182F>
 13. Teng, J., Liao, P., Wang, M.: The role of emerging micro-scale vegetables in human diet and health benefits—an updated review based on microgreens. *Food Funct.* 12, 1914–1932 (2021). <https://doi.org/10.1039/D0FO03299A>
 14. Hooshmand, K., Fomsgaard, I.S.: Analytical Methods for Quantification and Identification of Intact Glucosinolates in Arabidopsis Roots Using LC-Qq(LIT)-MS/MS. *Metabolites*. 11, 47 (2021). <https://doi.org/10.3390/metabo11010047>
 15. Capriotti, A.L., Cavaliere, C., La Barbera, G., Montone, C.M., Pivovesana, S., Zenezini Chiozzi, R., Laganà, A.: Chromatographic column evaluation for the untargeted profiling of glucosinolates in cauliflower by means of ultra-high performance liquid chromatography coupled to high resolution mass spectrometry. *Talanta*. 179, 792–802 (2018). <https://doi.org/10.1016/j.talanta.2017.12.019>
 16. Bianco, G.; Pascale, R.; Lelario, F.; Bufo, S.A.; Cataldi, T.R.I.: The investigation of glucosinolates by mass spectrometry. In: Merillon, J.M.; Ramawat, K. (eds): *Glucosinolates, Reference Series in Phytochemistry*, 2017, Springer, Cham (Switzerland) pp. 431–461. https://doi.org/10.1007/978-3-319-26479-0_12-1
 17. Rochfort, S.J., Trenery, V.C., Imsic, M., Panozzo, J., Jones, R.: Class targeted metabolomics: ESI ion trap screening methods for glucosinolates based on MSⁿ fragmentation. *Phytochemistry*. 69, 1671–1679 (2008). <https://doi.org/10.1016/j.phytochem.2008.02.010>
 18. Agerbirk, N., Pattison, D.I., Mandakova, T., Lysak, M.A., Montaut, S., Staerk, D.: Ancient Biosyntheses in an Oil Crop: Glucosinolate Profiles in *Limnanthes alba* and Its Relatives (Limnathaceae, Brassicales). *J. Agric. Food Chem.* 70, 1134–1147 (2022). <https://doi.org/10.1021/acs.jafc.1c07299>
 19. Liang, X., Lee, H.W., Li, Z., Lu, Y., Zou, L., Ong, C.N.: Simultaneous Quantification of 22 Glucosinolates in 12 Brassicaceae Vegetables by Hydrophilic Interaction Chromatography–Tandem Mass Spectrometry. *ACS Omega*. 3, 15546–15553 (2018). <https://doi.org/10.1021/acs.omega.8b01668>
 20. Erngren, I., Nestor, M., Pettersson, C., Hedeland, M.: Improved Sensitivity in Hydrophilic Interaction Liquid Chromatography–Electrospray–Mass Spectrometry after Removal of Sodium and Potassium Ions from Biological Samples. *Metabolites*. 11, 170 (2021). <https://doi.org/10.3390/metabo11030170>
 21. Dong, M., Tian, Z., Ma, Y., Yang, Z., Ma, Z., Wang, X., Li, Y., Jiang, H.: Rapid screening and characterization of glucosinolates in 25 Brassicaceae tissues by UHPLC-Q-exactive orbitrap-MS. *Food Chem.* 365, 130493 (2021). <https://doi.org/10.1016/j.foodchem.2021.130493>
 22. Geng, J., Xiao, L., Chen, C., Wang, Z., Xiao, W., Wang, Q.: An integrated analytical approach based on enhanced fragment ions interrogation and modified Kendrick mass defect filter data mining for in-depth chemical profiling of glucosinolates by ultra-high-pressure liquid chromatography coupled with Orbitrap high. *J. Chromatogr. A*. 1639, 461903 (2021). <https://doi.org/10.1016/j.chroma.2021.461903>
 23. Ventura, G., Bianco, M., Calvano, C.D., Losito, I., Cataldi, T.R.I.: HILIC-ESI-FTMS with All Ion Fragmentation (AIF) Scans as a Tool for Fast Lipidome Investigations. *Molecules*. 25, 2310 (2020). <https://doi.org/10.3390/molecules25102310>
 24. Schymanski, E.L., Jeon, J., Gulde, R., Fenner, K., Ruff, M., Singer, H.P., Hollender, J.: Identifying Small Molecules via High Resolution Mass Spectrometry: Communicating Confidence. *Environ. Sci. Technol.* 48, 2097–2098 (2014). <https://doi.org/10.1021/es5002105>
 25. De Ceglie, C., Calvano, C.D., Zamboni, C.G.: Determination of Hidden Hazelnut Oil Proteins in Extra Virgin Olive Oil by Cold Acetone Precipitation Followed by In-Solution Tryptic Digestion and MALDI-TOF-MS Analysis. *J. Agric. Food Chem.* 62, 9401–9409 (2014). <https://doi.org/10.1021/jf504007d>
 26. Blazevic, I., Montaut, S., Burcul, F., Olsen, C.E., Burow, M., Rollin, P., Agerbirk, N.: Glucosinolate structural diversity, identification, chemical synthesis and metabolism in plants. *Phytochem.* 169, 112100 (2020). <https://doi.org/10.1016/j.phytochem.2019.112100>
 27. Bialecki, J.B., Ruzicka, J., Weisbecker, C.S., Haribal, M., Attygalle, A.B.: Collision-induced dissociation mass spectra of glucosinolate anions. *J. Mass Spectrom.* 45, 272–283 (2010). <https://doi.org/10.1002/jms.1711>
 28. Attygalle, A.B., García-Rubio, S., Ta, J., Meinwald, J.: Collisionally-induced dissociation mass spectra of organic sulfate anions. *J. Chem. Soc. Perkin Trans. 2*. 498–506 (2001). <https://doi.org/10.1039/b009019k>
 29. Pino, L.K., Searle, B.C., Bollinger, J.G., Nunn, B., MacLean, B., MacCoss, M.J. The Skyline ecosystem: Informatics for quantitative mass spectrometry proteomics. *Mass Spectr. Rev.* 39, 229 (2017). <https://doi.org/10.1002/mas.21540>
 30. Clarke, D.B.: Glucosinolates, structures and analysis in food. *Anal. Methods*. 2, 310 (2010). <https://doi.org/10.1039/b9ay00280d>
 31. Lelario, F., Bianco, G., Bufo, S.A., Cataldi, T.R.I.: Establishing the occurrence of major and minor glucosinolates in Brassicaceae by LC–ESI-hybrid linear ion-trap and Fourier-transform ion cyclotron resonance mass spectrometry. *Phytochemistry*. 73, 74–83 (2012). <https://doi.org/10.1016/j.phytochem.2011.09.010>
 32. Maldini, M., Baima, S., Morelli, G., Scaccini, C., Natella, F.: A liquid chromatography-mass spectrometry approach to study “glucosinoloma” in broccoli sprouts. *J. Mass Spectr.* 47, 1198–1206 (2012). <https://doi.org/10.1002/jms.3028>
 33. Reva, I.; Lapinski, L.; Lopes Jesus, A.J.; Nowak, M.J.: Photoinduced transformations of indole and 3-formylindole monomers isolated in low-temperature matrices. *J. Chem. Phys.* 147, 194304 (2017). <https://doi.org/10.1063/1.5003326>
 34. Bianco, G., Agerbirk, N., Losito, I., Cataldi, T.R.I.: Acylated glucosinolates with diverse acyl groups investigated by high resolution mass spectrometry and infrared multiphoton dissociation. *Phytochemistry*. 100, 92–102 (2014). <https://doi.org/10.1016/j.phytochem.2014.01.010>

All ion fragmentation analysis enhances the untargeted profiling of glucosinolates in Brassica microgreens by liquid chromatography and high-resolution mass spectrometry

Andrea Castellaneta¹, Ilario Losito^{1,2,*}, Giovanni Cisternino¹, Beniamino Leoni³, Pietro Santamaria^{2,3}, Cosima Damiana Calvano^{1,2}, Giuliana Bianco⁴, Tommaso R.I. Cataldi^{1,2}

¹Dipartimento di Chimica, ²Centro Interdipartimentale SMART, ³Dipartimento di Scienze Agro-Ambientali e Territoriali, Università degli Studi di Bari Aldo Moro, via Orabona 4, 70126 Bari, Italy; ⁴Dipartimento di Scienze, Università degli Studi della Basilicata, viale dell'Ateneo Lucano 10, 85100 Potenza, Italy.

Synopsis

The graphic describes how the extraction of signal intensity referred to the glucosinolate common fragment corresponding to sulphate radical anion $[\text{SO}_4]^-$ from spectra obtained during the RPLC-ESI-AIF-FTMS analysis of microgreen extracts was exploited, along with those related to other typical fragments, to recognize peaks (emphasized by the red colour) subsequently confirmed to be related to glucosinolates.

